Seasonal variations of stratospheric age spectra in the Goddard Earth Observing System Chemistry Climate Model (GEOSCCM)

Feng Li,[1,2] Darryn W. Waugh,[3] Anne R. Douglass,[2] Paul A. Newman,[2] Steven Pawson,[2] Richard S. Stolarski,[2,3] Susan E. Strahan,[1,2] and J. Eric Nielsen[2,4]

Received 14 September 2011; revised 18 January 2012; accepted 23 January 2012; published 15 March 2012.

[1] The stratospheric age spectrum is the probability distribution function of the transit times since a stratospheric air parcel had last contact with a tropospheric boundary region. Previous age spectrum studies have focused on its annual mean properties. Knowledge of the age spectrum's seasonal variability is very limited. In this study, we investigate the seasonal variations of the stratospheric age spectra using the pulse tracer method in the Goddard Earth Observing System Chemistry Climate Model (GEOSCCM). The relationships between the age spectrum and the boundary impulse response (BIR) are reviewed, and a simplified method to reconstruct seasonally varying age spectra is introduced. The age spectra in GEOSCCM have strong seasonal cycles, especially in the lowermost and lower stratosphere and in the subtropical overworld. These changes reflect the seasonal evolution of the Brewer-Dobson circulation, isentropic mixing, and transport barriers. We also investigate the seasonal and interannual variations of the BIRs. Our results clearly show that computing an ensemble of seasonally dependent BIRs is necessary in order to capture the seasonal and annual mean properties of the stratospheric age spectrum.

Citation: Li, F., D. W. Waugh, A. R. Douglass, P. A. Newman, S. Pawson, R. S. Stolarski, S. E. Strahan, and J. E. Nielsen (2012), Seasonal variations of stratospheric age spectra in the Goddard Earth Observing System Chemistry Climate Model (GEOSCCM), *J. Geophys. Res.*, *117*, D05134, doi:10.1029/2011JD016877.

1. Introduction

[2] The mean age of stratospheric air is the average time for an air parcel to travel from a source region in the troposphere (or near the tropopause) to a sample region in the stratosphere [*Hall and Plumb*, 1994]. The mean age is a fundamental transport time scale that has been widely used in stratospheric transport studies, particularly in the evaluation of chemical transport models and chemistry-climate models (CCMs) [*Hall et al.*, 1999a, 1999b; *Eyring et al.*, 2006]. However, the mean age only contains partial information of transit time scales. The complete information is included in the age spectrum, i.e., a probability distribution function of all the possible transit times since an air parcel had last contact with the tropospheric boundary source region [*Hall and Plumb*, 1994; *Waugh and Hall*, 2002]. Many studies have shown that the age spectrum is more useful than the mean age in diagnosing transport characteristics, e.g., the relative importance of different transport pathways into the lower stratosphere [*Andrews et al.*, 2001a; *Bönisch et al.*, 2009], the seasonal variations of stratospheric transport [*Andrews et al.*, 1999, 2001b; *Reithmeier et al.*, 2008; *Bönisch et al.*, 2009], and the horizontal recirculation rate in the tropical pipe region [*Strahan et al.*, 2009].

[3] The age spectrum is a kind of boundary propagator. By definition, the boundary propagator $G(r,t\ \Omega,t)$ is a Green's function that solves the continuity equation for the mixing ratio of a conserved and passive tracer $\chi(r,t)$ [*Hall and Plumb*, 1994]. If the mixing ratio is uniform on the boundary source region Ω, this solution can be expressed by the following integration

$$\chi\ r,t \quad \int^{t} \chi\ \Omega,t\ \ G\ r,t\ \Omega,t\ \ dt\ ,$$

where r is the sample region, t is the source time or the time the tracer had last contact with Ω, and t is the field time or the time the tracer is sampled at r. In many cases the boundary propagator is easier to interpret if it is rewritten as a function of the transit time $\xi = t \quad t$, i.e.,

$$\chi\ r,t \quad \int_{0} \chi\ \Omega,t \quad \xi\ G\ r,t\ \Omega,t \quad \xi\ d\xi,$$

where $G(r,t\ \Omega,t \quad \xi)d\xi$ represents the mass fraction of the air parcel at r and a specific field time t that was last in contact

[1]Goddard Earth Sciences Technology and Research, Universities Space Research Association, Columbia, Maryland, USA.
[2]NASA Goddard Space Flight Center, Greenbelt, Maryland, USA.
[3]Department of Earth and Planetary Science, Johns Hopkins University, Baltimore, Maryland, USA.
[4]Science Systems and Application Inc., Lanham, Maryland, USA.

0148-0227/12/2011JD016877

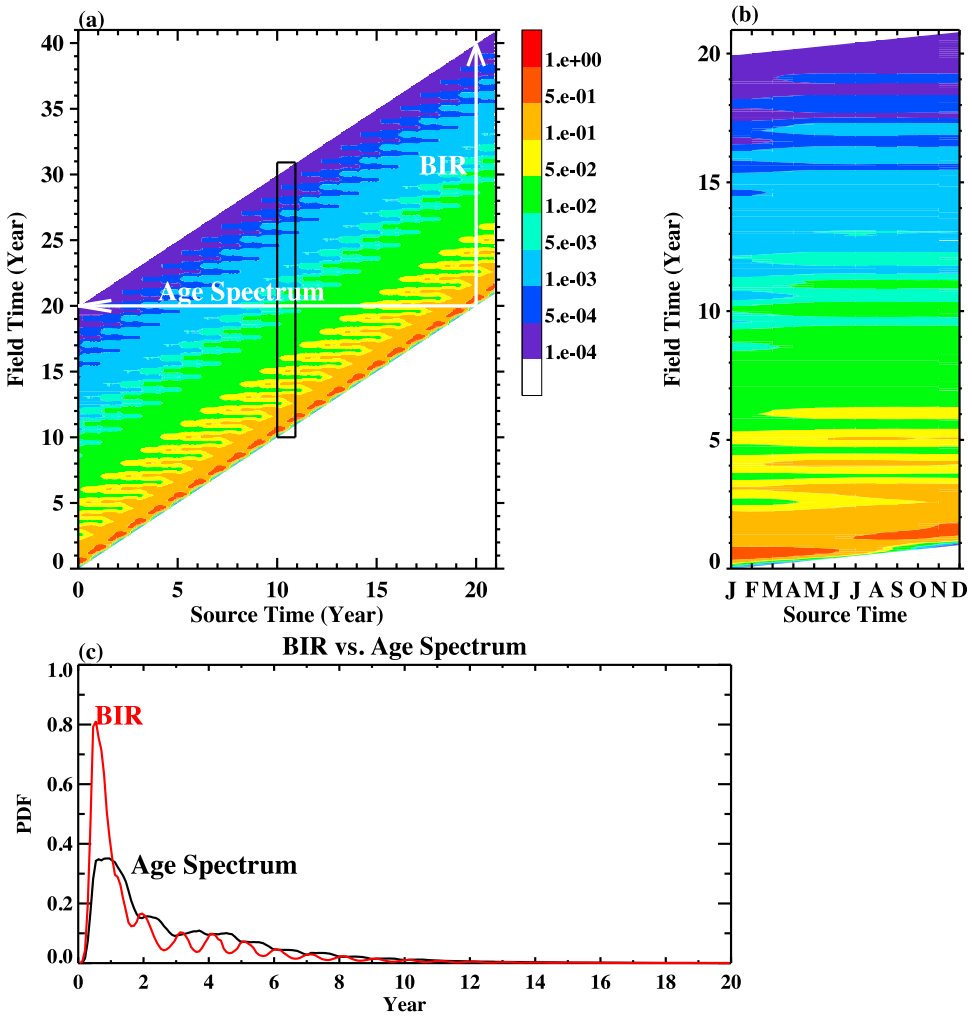

Figure 1. Illustration of the relationship between the age spectrum and boundary impulse response (BIR). (a) Boundary propagator map at 60°N and 420 K. This map is constructed from 252 vertical slices. Each vertical slice is a BIR, which is fixed in source time and increases with field time. The age spectrum is fixed in field time and increases toward older source time, i.e., a horizontal cut from right to left through the boundary propagator map. (c) An example of the BIR and age spectrum. When constructing the boundary propagator map of Figure 1a, we do not calculate all the 252 BIRs. Instead, we only calculate 12 BIRs with source time in each month of a given year. These 12 BIR realizations (shown in Figure 1b and in the black rectangle in Figure 1a) are then repeated every year for 20 years to form the boundary propagator map.

with Ω between ξ and $\xi + d\xi$ ago [*Waugh and Hall*, 2002; *Holzer et al.*, 2003; *Haine et al.*, 2008]. Here $G(r,t|\Omega,t-\xi)$ is the age spectrum, which is also called the transit time distribution (TTD) in tropospheric and ocean transport literatures [e.g., *Holzer et al.*, 2003; *Haine et al.*, 2008]. In this paper we follow the stratospheric terminology and use age spectrum to refer $G(r,t|\Omega,t-\xi)$.

[4] The age spectrum cannot be directly observed, and we rely almost solely on models to compute it. Several methods have been used to calculate the age spectrum, e.g., the Eulerian pulse tracer method [*Hall et al.*, 1999b], the Lagrangian trajectory method [*Schoeberl et al.*, 2003], and the Eulerian adjoint model method [*Haine et al.*, 2008]. The age spectrum can also be obtained empirically by fitting an assumed analytic form of the age spectrum with tracer measurements [e.g., *Andrews et al.*, 1999; *Waugh et al.*, 2003, 2004; *Schoeberl et al.*, 2005; *Khatiwala et al.*, 2009].

[5] The pulse tracer method has been used more commonly than other methods because it is the most direct approach and is easy to implement. A pulse of a conserved and passive tracer is placed in the boundary source region Ω at a specific source time t′ where it disperses throughout the interior volume. The time series of the mixing ratio of this tracer at any interior point r, which can be expressed mathematically as $G(r,t'+\xi|\Omega,t')$, represents the model's time-evolving response to a delta function boundary condition. $G(r,t'+\xi|\Omega,t')$ is called the boundary impulse response (BIR) [*Haine et al.*, 2008]. Thus the direct product of the pulse tracer method is not the age spectrum, but the BIR. In general the BIR $G(r,t'+\xi|\Omega,t')$ is not equal to the age spectrum $G(r,t|\Omega,t-\xi)$.

[6] The relationship between the age spectrum and the BIR is illustrated in Figure 1a, which is an example of the boundary propagator map at 60°N and 420 K isentropic surface. The age spectrum and the BIR are perpendicular to

each other in the boundary propagator map. The age spectrum is fixed in field time and increases toward older source time, i.e., a horizontal cut through the boundary propagator map from right to left. The BIR is fixed in source time and increases with field time, i.e., a vertical slice from bottom to top. For unsteady flow the boundary propagator is a function of both field time t and source time t and therefore the age spectrum and the BIR are not the same (Figure 1c). However, if the flow is steady, at least in a statistical sense, the boundary propagator is only a function of the transit time ξ, i.e., for any t and t , $G(r,t\ \Omega,t\quad \xi) = G(r,t+\xi\ \Omega,t)$; that is, in steady flow the age spectrum and the BIR are the same. Previous stratospheric pulse tracer age spectrum studies have made the assumption of stationarity to compute the age spectrum from the BIR [*Hall and Plumb*, 1994; *Hall et al.*, 1999a, 1999b; *Schoeberl et al.*, 2005]. These studies assumed steady flow in the sense that the seasonal variations of the BIR and age spectrum can be ignored and performed a single realization of the BIR as an approximation of the annual-mean or time-averaged age spectrum.

[7] The traditional stratospheric pulse tracer studies have greatly improved our understanding of the annual mean properties of the age spectrum [*Hall and Plumb*, 1994; *Waugh and Hall*, 2002; *Schoeberl et al.*, 2005], but their approach has disadvantages. By assuming steady flow and performing a single realization, their method cannot be used to investigate the seasonality of the stratospheric age spectra. Stratospheric transport has a strong seasonal cycle due to the seasonal variations of processes such as tropical upwelling, subtropical jets, and polar vortices [e.g., *Chen*, 1995; *Pan et al.*, 1997; *Rosenlof et al.*, 1997; *Ray et al.*, 1999; *Randel et al.*, 2001]. One would expect the stratospheric age spectra to have large seasonal variations. However, our knowledge of the age spectrum's seasonality is very limited. To date the only work that investigated the seasonal variations of stratospheric age spectra was done by *Reithmeier et al.* [2008] using a Lagrangian trajectory method. *Reithmeier et al.* [2008] found that the age spectra in the ECHAM4 general circulation model (GCM) have strong seasonal cycles, and that the shapes of the age spectra change significantly with latitudes. However, there are serious transport biases in ECHAM4. Specifically, the subtropical barrier is too weak and is located too far away from the equator compared to observations. These biases could be related to the limitations of the version of ECHAM4 used by *Reithmeier et al.* [2008], which has a very coarse horizontal (6) and vertical (only 19 levels) resolution and a very low model top at 10 hPa. The model limitations and the poor transport performance cast doubts on the results of *Reithmeier et al.* [2008].

[8] Another concern about the traditional pulse tracer method is whether a single BIR is a good approximation of an annual-mean age spectrum. Because in reality the stationary assumption does not hold, the single BIR approach implies that the seasonality of stratospheric transport has small impact on the annual mean properties of the age spectrum. *Hall et al.* [1999b] found that the mean age of a single BIR agrees reasonably well with the annually averaged clock tracer mean age. This was used as evidence that the annual mean properties of the age spectrum could be well captured by a single BIR realization. But no previous studies actually investigated the seasonal change of the BIR and the differences between the age spectrum and the BIR in the stratosphere.

[9] The limits of the traditional stratospheric pulse tracer method can be addressed by performing an ensemble of time-dependent BIR simulations. *Holzer et al.* [2003] and *Haine et al.* [2008] described in detail a straightforward method to calculate the age spectra in unsteady flow using the pulse tracer. We will review their method in the next section. This method requires performing a large number of BIR experiments in different seasons and years to reconstruct the time-varying age spectra, and therefore it is computationally expensive.

[10] In this study we investigate the seasonal variations of the age spectra in the Goddard Earth Observing System Chemistry-Climate Model (GEOSCCM) using the pulse tracer method. We introduce an approach to significantly reduce the computational cost for calculating seasonally varying age spectra based on the method of *Holzer et al.* [2003] and *Haine et al.* [2008]. Our main purpose is to understand the seasonality of the stratospheric age spectra. Another purpose is to clarify the differences between the BIR and the age spectrum. Our work broadens the usage of the pulse tracer age spectra. These results will improve the understanding of the transport characteristics in the GEOSCCM, which has been shown to produce realistic stratospheric transport by various diagnostics [*Strahan et al.*, 2011]. Our results could also be used by empirical studies as guidance for age spectrum's seasonal variability.

[11] Our method for calculating the age spectra is described in section 2. We describe how to compute age spectra and BIRs in unsteady flow using a simplified version of the method of *Holzer et al.* [2003] and *Haine et al.* [2008]. We also briefly introduce the GEOSCCM and the simulations. In section 3 we discuss the seasonal and interannual variations of the BIRs. Seasonal variations of the age spectra are presented in section 4. Discussions and summary are given in section 5. All results presented in this paper are zonally and monthly averaged and then interpolated to the isentropic coordinate.

2. Method

[12] As introduced in section 1, the BIR can be easily computed from the pulse tracer experiment. Once the BIR is obtained, the age spectrum can be constructed from a series of BIRs. For steady flow, this is simple because the age spectrum equals the BIR. We need only perform a single tracer experiment because the age spectrum for a stationary condition has no time dependence. But in reality, transport is not stationary and computing the age spectrum is more complicated. The most direct method is to construct a complete boundary propagator map with many successive vertical BIR sections and then a horizontal cut through the map gives the age spectrum (Figure 1) [see also *Haine et al.*, 2008, Figure 1; *Holzer et al.*, 2003, Figure 2]. This method requires a large number of tracer experiments, so in practice some simplifications have to be made.

[13] We first compute 12 BIRs with 12 pulse tracers released in each month of a given model year. The method of *Hall et al.* [1999b] is followed to compute the BIR. The boundary source region is set to be the tropical lower troposphere from 10 S to 10 N and between the surface and about

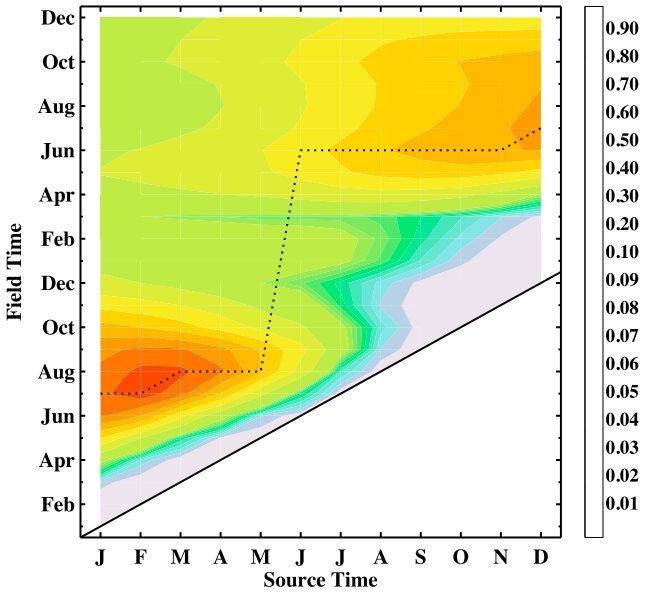

Figure 2. Seasonal evolution of the BIRs at 80 N and 420 K as a function of source time and field time. The dotted line indicates the time of the peaks of the BIRs.

800 hPa. In order to approximate the delta function boundary condition, a pulse of artificial conserved and passive tracer is uniformly released in the source region. The tracer's mixing ratio is set to an arbitrary constant value for the first month of the experiment and then held as zero through the rest of the experiment in the source region. Each experiment runs for 20 years in order to account for the long tail of the stratospheric age spectrum [*Schoeberl et al.*, 2003]. Then the time series of the tracer's mixing ratio is the BIR. Figure 1b shows an example of the calculated BIRs at 60 N and 420 K as a function of source time t and field time t. Here the source time represents when the pulses are released at the tropical surface and the field time is when the mixing ratio of the tracer is sampled in the stratosphere.

[14] The 12 BIRs form 12 vertical sections of the boundary propagator map, but they are not enough to reconstruct the age spectra. For a 20-year-long age spectrum, a total of 240 pulse experiments are needed. In practice it is not possible to run such a large number of experiments with the GEOSCCM. So we make an initial assumption that the BIR's interannual variability is sufficiently small compared to its seasonal variability that we can ignore age spectrum's interannual variations for the purpose of this study. We will show in section 3 that this assumption of cyclostationarity is reasonable in the GEOSCCM. Under this assumption, we construct the boundary propagator map by repeating the 12 BIRs every year for 20 years and shifting the source time accordingly, i.e., let $G(r,t + \xi\ \Omega,t) = G(r,t + \xi + n \quad 12\ \Omega,t + n \quad 12)$, where t = Jan, Feb,…, Dec represents the source time of the pulse tracer experiments, and n = 1, 20 are the repeating years. We then obtain the age spectra as horizontal cuts through the map (Figure 1a). In the next section we show evidence that our method is valid in a climatological mean sense, i.e., our calculation captures very well the seasonality of the climatological mean. Note the GEOSCCM does not produce a quasibiennial oscillation (QBO). If the model generates a QBO, we would need to use more than 1 year of BIRs to compute the age spectra.

[15] The pulse experiments were performed in a transient simulation using the GEOSCCM Version 2. The GEOSCCM Version 2 is an update from the GEOSCCM version 1 [*Pawson et al.*, 2008]. It couples the GEOS5-GCM [*Rienecker et al.*, 2008] with a comprehensive stratospheric chemistry package [*Douglass et al.*, 1996]. The model has 72 vertical levels with a top level at 0.01 hPa. The simulation was carried out on a horizontal resolution of 2 latitude by 2.5 longitude. The 12 pulses were released in each month of model year 2000 and were integrated for 20 years to 2019, where the model year represents the conditions of the external forcings. The simulation was forced with *Intergovernmental Panel on Climate Change* [2001] greenhouse gas (GHG) scenario A1b and *World Meteorological Organization* [2007] ozone depleting substance scenario A1. The sea surface temperature and sea ice contents were taken from an NCAR Community Climate System Model 3.0 run in the A1b GHG scenario. The solar forcing was held constant in the experiments.

[16] Results from the GEOSCCM Version 2 have been extensively analyzed and evaluated using observation-based process-oriented diagnostics along with other CCMs in the SPARC CCMVal-2 project (http://www.atmosp.physics.utoronto.ca/SPARC). Overall the GEOSCCM performs well in terms of the mean stratospheric dynamical and thermal structure, trace gas distributions, and their decadal changes in the recent past. The GEOSCCM also simulates well the extratropical interannual variability, such as the frequency of stratospheric sudden warmings and the variations of the polar jets. The model underestimates the tropical interannual variability, however, because it does not produce a QBO. The GEOSCCM has quite realistic transport characteristics in the stratosphere. It has the best performance in mean age among all the CCMs that participated in the CCMVal-2. Lacking a QBO does not appear to have a big impact on the model's ability to capture the mean tropical transport characteristics. The tropical ascent rates and the subtropical lower stratospheric mixing rates compare well to observations [*Strahan et al.*, 2011]. But the GEOSCCM has a somewhat stronger subtropical barrier in the middle stratosphere and a stronger Antarctic polar vortex barrier than observed.

3. Seasonal and Interannual Variations of the Boundary Impulse Responses

[17] A concern about the traditional pulse tracer approach is that it uses only a single BIR realization to approximate the annual-mean age spectrum. *Haine et al.* [2008] showed theoretically that the statistical properties of an ensemble mean of the age spectra are equivalent to those of an ensemble mean of the BIRs in unsteady flow. We have compared the annual-mean age spectra and BIRs in our model simulations and have found they are nearly identical (not shown). This means if the seasonality of the BIR is small, a single BIR realization could be a good representation of an annual-mean age spectrum.

[18] However, our simulations show significant seasonal variations in the BIRs. As an example, Figure 2 plots the seasonal evolution of the BIRs at 80 N and 420 K. This is

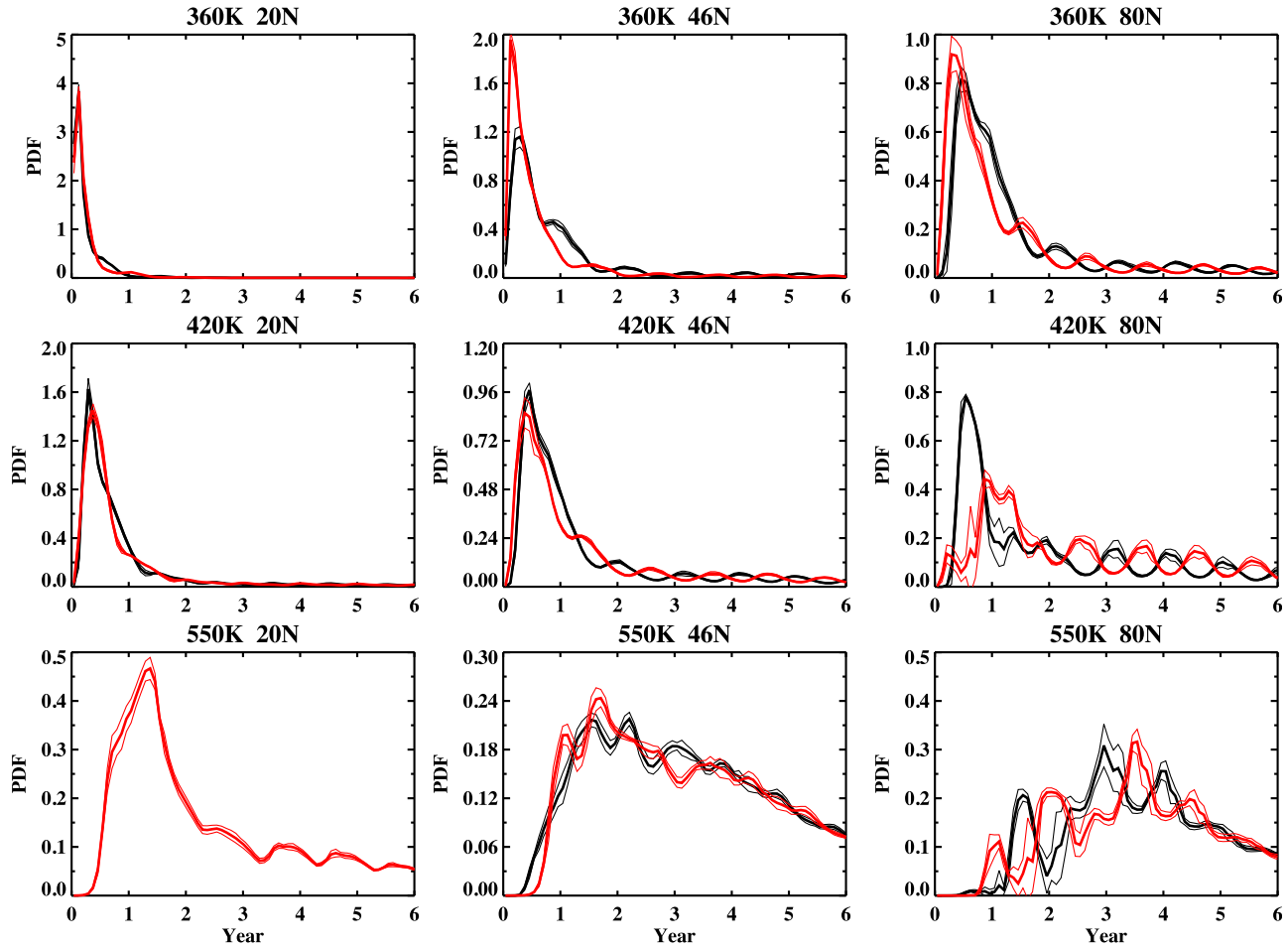

Figure 3. Comparison of the January (black) and July (red) BIRs at some chosen locations in the Northern Hemisphere. The bold lines are the mean of five BIRs, which are released in January or July 2000–2004. The thin lines are the standard deviations of the five BIRs.

similar to Figure 1b, but only the first 2 years of the BIRs are shown. Figure 2 shows that the BIRs released in winter–early spring have stronger and younger peaks than those released in summer–early fall. The most interesting feature is that the peaks of the BIRs are seasonally locked to the summer field time. No matter when the pulse is released, its peak always reaches high latitudes during June–August. It takes about 6 months for the peaks of the winter-released pulse to arrive 80 N. The transport of summer-released BIRs into the polar lower stratosphere is strongly suppressed in winter and early spring by the vortex barrier. They do not penetrate into the high latitudes until the breakup of the polar vortex in late spring. This leads to the oldest and weakest peaks. The large seasonal variations of the BIRs shown in Figure 2 clearly demonstrate that the annual-mean properties of the age spectrum cannot be well captured by a single BIR in areas such as the polar region.

[19] We also want to emphasize that the seasonal change of the BIR, which is based on the source time, could be very different from the seasonal change of the age spectrum that is based on the field time. In Figure 2, the summer–early fall peaks and winter–early spring valleys with respect to the field time means that the age spectra, which are horizontal cuts from right to left through the boundary propagator map, have younger, stronger peaks and a narrower shape in summer–early fall than in winter–early spring. Thus the seasonal cycle of the age spectra is nearly out of phase with that of the BIRs in the Arctic lower stratosphere.

[20] We made an initial assumption that the BIR's interannual variations are smaller than its seasonal variations. We performed eight additional pulse experiments to verify that this assumption is valid. The eight pulses were released in January and July in years 2001 to 2004, respectively. Since we already have the January and July BIR for year 2000, a total of five January-released and five July-released BIRs for 2000–2004 were obtained. The mean and standard deviations of the five January (black) and July (red) BIRs at some chosen locations in the Northern Hemisphere (NH) are shown in Figure 3. The Southern Hemisphere (SH) has very similar features and is not shown. In the subtropical lower stratosphere (20 N at 360 K and 420 K) the interannual variations are very small such that the lines representing the standard deviation almost overlap with the mean BIR. In the midlatitude lower stratosphere the magnitude of the spectral peaks shows some interannual variations. Considerable interannual changes are found in the 550 K extratropics

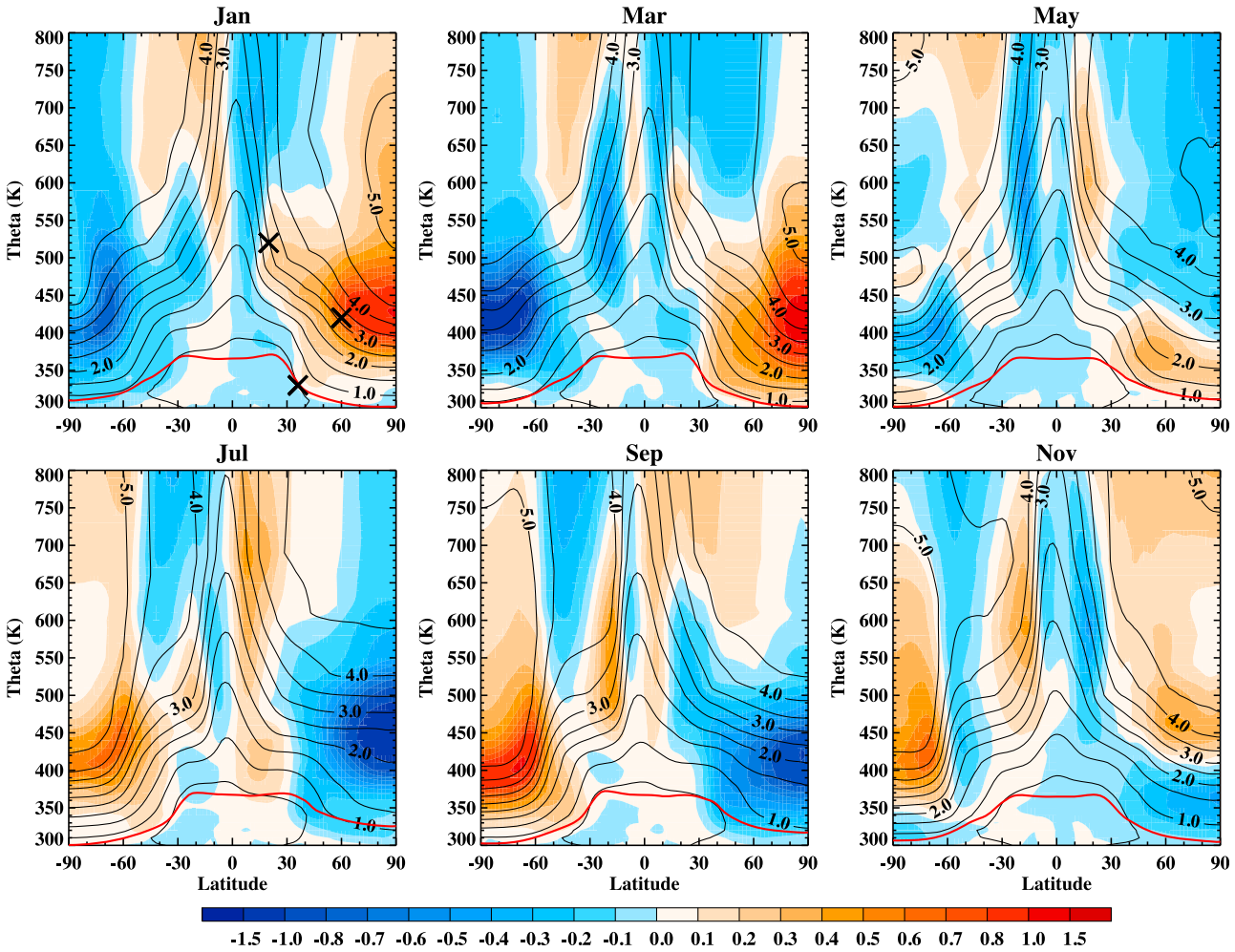

Figure 4. Distribution of the age spectrum mean age (lines) and its difference from the annually averaged mean age (color) at 2 month intervals. The contour interval is 0.5 years. The red line is the tropopause. The cross symbol for January indicates the location of the transport barriers.

and polar lower stratosphere. Nevertheless, the seasonal differences between the January and July BIRs clearly stand out.

[21] The cyclostationarity assumption might also be affected by the secular trend in the stratospheric transport due to increases in GHGs. But this is not an important factor in our short 20 year integration. We have calculated the linear trend in the annually averaged clock tracer mean age and found that the trend is not statistically significant in most of the stratosphere.

4. Seasonal Variations of the Age Spectra

[22] Three parameters that characterize aspects of the age spectra are the modal age $\tau_M(r, t)$, the mean age $\Gamma(r, t)$, and the width $\Delta(r, t)$ [*Waugh and Hall*, 2002]. The modal age is the most probable transit time, corresponding to the time of the spectral peak. The mean age is the first moment of the age spectrum $\Gamma(r,t) = \int_0^\infty \xi G(r,t|\Omega, t-\xi)d\xi$ and represents the average transit time. The width is related to the second moment of the age spectrum $\Delta(r,t) = \sqrt{1/2\int_0^\infty (\xi - \Gamma(r|t))^2 G(r,t|\Omega, t-\xi)d\xi}$, which is a measure of the spread of the spectrum. Among the three parameters, only the mean age's seasonal variability has been studied before [*Andrews et al.*, 1999, 2001b; *Reithmeier et al.*, 2008; *Bönisch et al.*, 2009]. In this study, we explore the seasonal variations of all three parameters, but first focus on the mean age.

[23] Figure 4 shows the mean age (lines) and its differences from the annually averaged mean age (color) as functions of latitude and potential temperature at 2 month intervals. The mean age has significant seasonal variations and these variations change with latitude and height (also see Figures 7a, 7d, and 7g which show the seasonal evolution of the mean age at the 360 K, 420 K, and 550 K isentropic surface). In the extratropical lower stratosphere (poleward of about 30° latitude and below about the 500 K isentropic surface), the mean age has a strong annual cycle with the youngest air in summer and early fall and the oldest air in winter and early spring. Large seasonal change is also found in the subtropical lower stratosphere (between 10° and 30° latitude and below about 450 K). Its magnitude is smaller than that in the extratropics

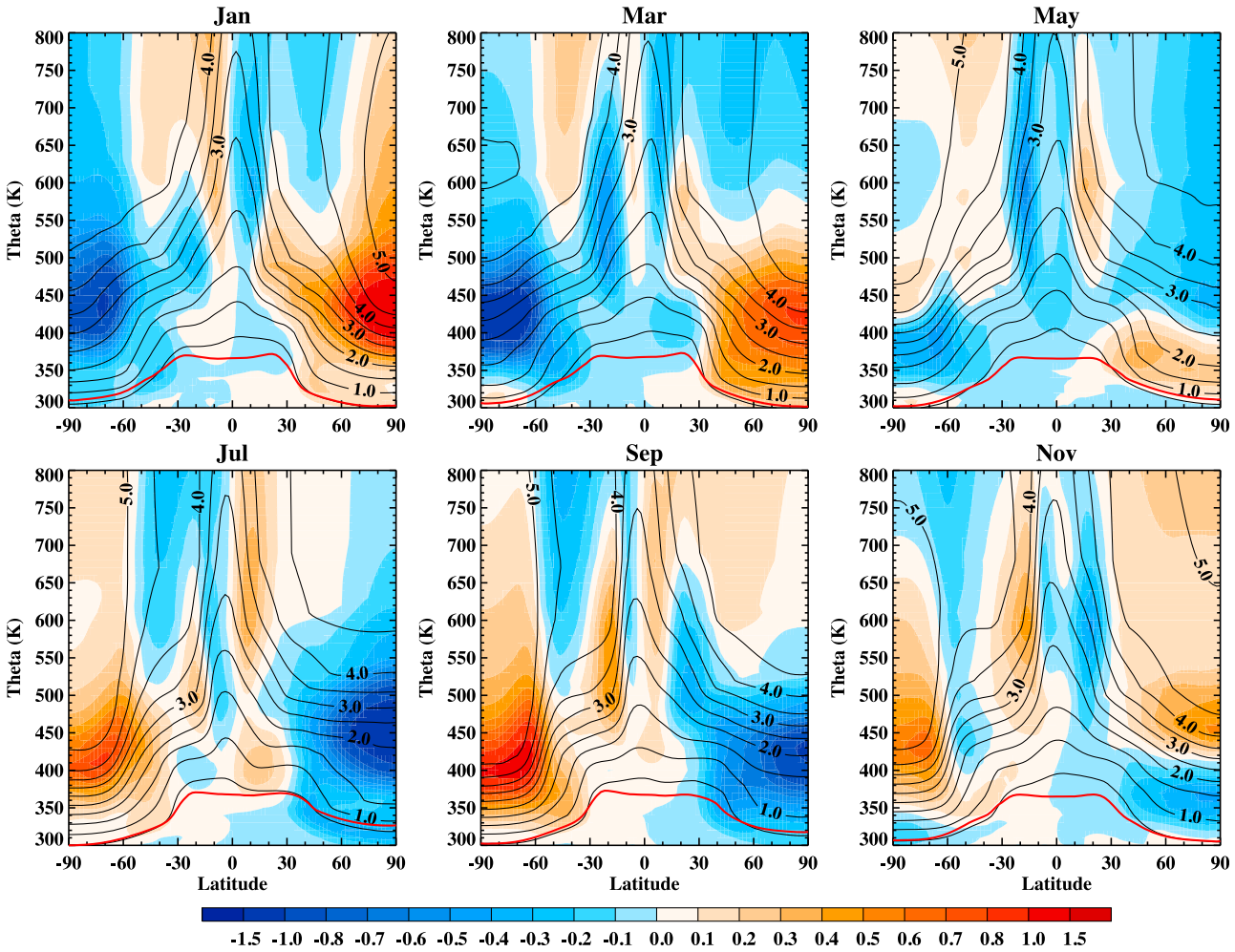

Figure 5. Same as Figure 4 but for the climatological mean clock tracer mean age.

in absolute value, but is comparable in relative change, which is up to 40% different from the annual-mean value. In winter–early spring and summer–early fall, the seasonal cycle in the subtropical lower stratosphere is nearly out of phase with that in the extratropics. In the middle and upper stratosphere above about 500 K the seasonal variability of the mean age is generally smaller than that in the lower stratosphere, and the largest seasonal variations are found in the subtropics.

[24] Before discussing the seasonal variations of the age spectra in more detail, we conduct a consistency check within the model by comparing the age spectrum mean age and its seasonal cycle with the model clock tracer mean age. The clock tracer is a linearly increasing tracer whose source region is at the global surface. For the clock tracer, the mean age is simply calculated as the time lag between the stratospheric sample region and the reference region, defined here as the tropical surface in order to be consistent with the pulse tracer experiment. This consistency check can determine whether our calculated age spectrum mean age is correct and whether it is worth investigating further into the seasonality of the age spectra. Figure 5 shows the climatology of the monthly clock tracer mean age distribution. Comparing Figure 5 with Figure 4 clearly shows that the clock tracer and age spectrum have almost exactly the same mean age distribution and seasonal variations. Small differences are found in the tropopause region. It appears that the clock tracer mean age is a bit younger and its seasonal cycle is stronger than the age spectrum mean age in the extratropical tropopause region. Nevertheless, given the completely different methodology in the age spectrum and the clock tracer, the overall very similar mean age seasonal evolution in these two methods provides convincing evidence that our calculation of the age spectrum is valid, in the sense it represents very well the climatological seasonal variations of the age spectra.

[25] The model simulated mean age seasonal variations agree well with the small number of observational studies that have been published to date. *Bönisch et al.* [2009] investigated this topic with mean age derived from in situ measurements of SF_6 and CO_2 during the SPURT aircraft campaigns that were carried out in the upper troposphere–lower stratosphere in the extratropics over Europe. They found that in the lowermost stratosphere bounded by the tropopause and the 380 K isentropic surface, the oldest air (>3 years) was observed in April and the youngest air (<1 year) was observed in October. Our model results are consistent with *Bönisch et al.* [2009], although the oldest air occurs in March and the youngest air occurs in September in our model calculations (note there are no March and

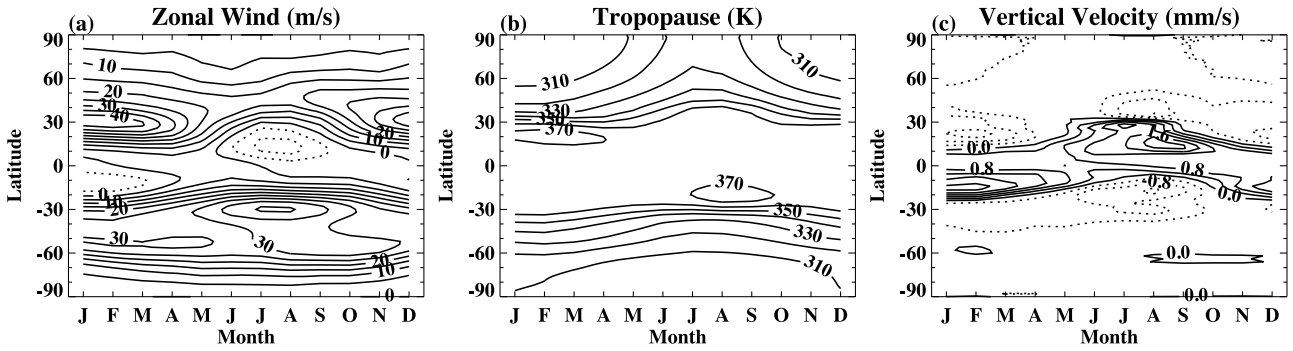

Figure 6. Seasonal cycle of (a) the zonal wind at 360 K, (b) the tropopause height, and (c) the residual vertical velocity at 360 K.

September data from *Bönisch et al.* [2009]). *Andrews et al.* [2001b] estimated the seasonal distribution of mean age in the lower stratosphere between about 380 K and 520 K from in situ N_2O measurements made by the NASA ER-2 aircraft during the period 1992–1998. Their estimation is based on the observed compact relationship between N_2O and mean age from ER-2 measurements. The estimated mean age distribution has relatively small uncertainties in the extratropics, but has large errors in the tropics-subtropics due to limited samplings of the ER-2 data in this region. In our model calculations the magnitude and phase of the seasonal cycle of mean age agree well with *Andrews et al.* [2001b] in the extratropical lower stratosphere. These agreements give us more confidence in our calculations.

[26] The seasonal change of the mean age reflects the seasonality of stratospheric transport. In a simplified view, the stratospheric transport is controlled by the integrated effects of the slow Brewer-Dobson circulation (with time scale of years) and the relatively fast isentropic mixing (with time scale of weeks to months). The Brewer-Dobson circulation is strongest in NH winter and weakest in NH summer [*Rosenlof*, 1995]. The impact of seasonal variations of isentropic mixing is dominated by seasonal evolution of the mixing barriers. There are three mixing barriers, which can be identified by the locations of the strongest gradients in Figure 4 (indicated by the cross). The polar barrier, located at the edge of the polar vortex in winter and early spring, suppresses mixing between the polar old air and midlatitude young air. The subtropical barrier isolates the tropical pipe from the surf zone in the overworld and it is strongest in late winter–early spring and weakest in late summer–early fall. The tropospheric jet or tropopause barrier significantly limits cross-tropopause mixing between the tropical upper troposphere and the midlatitude lowermost stratosphere in winter. The seasonal variations of the mean age are determined by these processes.

[27] The seasonal cycle of the mean age in the extratropical lowermost stratosphere (between about the tropopause and the 380 K isentropic surface) indicates that the fast isentropic mixing between the tropical upper troposphere or tropical tropopause layer (TTL) and the midlatitude lowermost stratosphere is most important in summer–early fall and least important in winter–early spring [*Bönisch et al.*, 2009]. This is consistent with the seasonal cycle of the tropical jet and tropopause barrier [*Chen*, 1995; *Pan et al.*, 1997]. The tropospheric jet is weak and the tropopause is high during the summer–early fall (Figures 6a and 6b), and the cross-tropopause isentropic mixing is strong. In winter–early spring the strong tropospheric jet and low tropopause height significantly suppress the cross-tropopause mixing. The strong wintertime and weak summertime Brewer-Dobson circulation descent may also play a role in determining the seasonal change of the mean age in the lowermost stratosphere.

[28] A very similar cycle is found in the extratropical lower stratosphere between about the 380 K and 500 K isentropic surface. Again this suggests that isentropic mixing has the largest impact and Brewer-Dobson circulation descent has the smallest impact in summer–early fall. In the polar stratosphere the seasonal evolution of the Brewer-Dobson circulation and the polar barrier determine the seasonal change of the mean age. In winter the strong descent brings old air to the polar region from higher altitudes. The polar barrier prohibits mixing between the old polar air and the young midlatitude air throughout the winter, resulting in the oldest air being found in spring in the polar region. In summer and early fall, mixing with the younger midlatitude air and weak descent result in the youngest polar air.

[29] It is interesting that the seasonal cycle of the mean age has nearly opposite phase between the subtropical and extratropical lower stratosphere below about the 450 K isentropic surface. This feature is most clearly seen in the NH in January, March, July, and September in Figure 4 (also see Figures 7a and 7d). The seasonal change of the subtropical lower stratospheric mean age cannot be explained by that of the tropical upwelling. The strongest upwelling occurs in the subtropics of the summer hemisphere (Figure 6c), but the oldest subtropical air is found in the summer hemisphere. Our explanation is that the opposite phase reflects the seasonally varying strength of the transport barrier in the subtropical lower stratosphere. In summer–early fall when transport is not restricted, strong mixing between the subtropics and midlatitudes leads to anomalously old subtropical air and young midlatitude air. In winter–early spring when transport is restricted, weak mixing leads to anomalously young subtropical air and old midlatitude air. This model feature is not clear in the mean age climatology of *Andrews et al.* [2001b]. But the mean age estimation of *Andrews et al.* [2001b] has large uncertainties in the tropical-subtropical lower stratosphere and more accurate mean age observations in this region are needed to verify our model results.

[30] We also note the phase of the seasonal cycle of the subtropical mean age changes above the 450 K isentropic

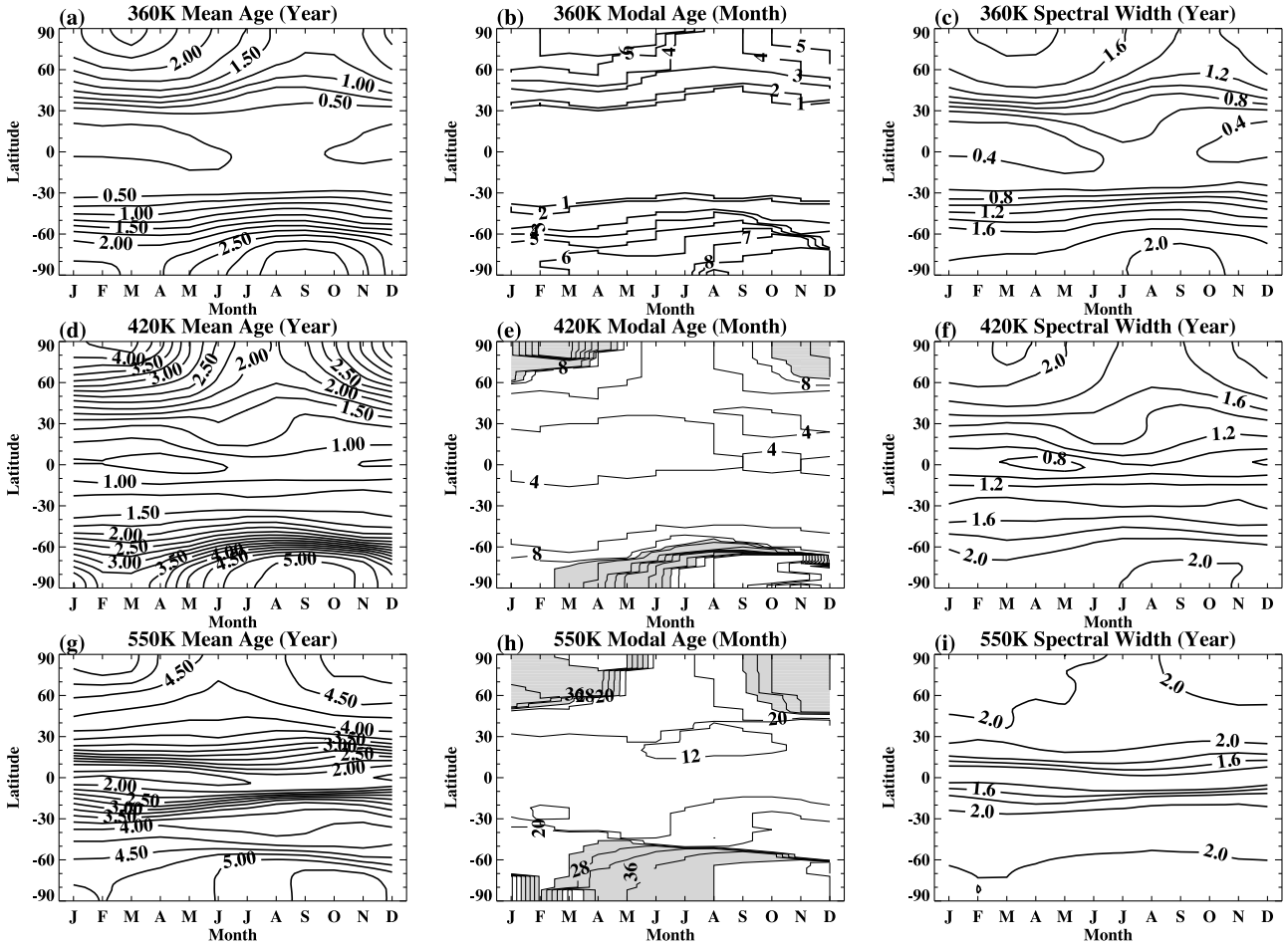

Figure 7. Seasonal evolution of the age spectrum mean age, modal age, and width at 360, 420, and 550 K. The contour interval is 0.25 years for the mean age and 0.2 years for the width. The unit of the modal age is month, and variable contour intervals are used in different levels: 1 month at 360 K, 2 months (modal age < 12 months) and 4 months (modal age > 12 months) at 420 K, and 4 months at 550 K. The shading in Figures 7e and 7h indicates regions of strong gradient in the modal age at 420 K (between 10 and 36 months) and 550 K (between 24 and 40 months).

surface, which is most clearly seen in winter–early spring and summer–early fall. This suggests the base of the tropical pipe is located at about 450 K, consistent with observations [*Rosenlof et al.*, 1997]. The edge of the lower tropical pipe moves toward the equator in late winter–early spring and brings old air to the subtropical lower stratosphere above 450 K. It moves away from the equator in late summer–early fall and the subtropical lower stratosphere is filled with more young tropical air. The seasonal variations of the location and strength of the subtropical barrier also regulate the mean age changes in the tropical pipe region between about 10°N and 10°S above 450 K. The subtropical barrier is located closer to the equator and is stronger in the winter hemisphere than in the summer hemisphere. This causes the mean age in the tropical pipe to be younger in winter than in summer.

[31] The age spectra provide additional information on transit time scales. Figure 7 shows the seasonal evolution of the modal age, width and the mean age at the 360, 420, and 550 K isentropic surfaces. Outside the tropics the 360 K isentropic surface represents the lowermost stratosphere. The 420 K isentrope is used to represent the tropically controlled transition region, which is bounded between approximately the 380 K and 450 K isentropic surfaces [*Rosenlof et al.*, 1997]; the 550 K is chosen to represent the overworld.

[32] The width is an important age spectrum parameter [*Hall and Plumb*, 1994]. Physically it is a measure of the strength of the recirculation, which depends on mixing across the transport barriers [*Strahan et al.*, 2009]. A stronger recirculation leads to a wider width, longer tail, and older mean of the spectra. Thus it is not surprising that the width has almost the same seasonal variations as the mean age. But the amplitude of the seasonal cycle of the width is smaller than that in the mean age, especially at high latitudes.

[33] The modal age represents the time scale of the most common path. Its seasonal change is similar to that of the mean age, but the modal age change is more abrupt. At 360 K the modal age is 1 month equatorward of 30°N and 30°S for all seasons. But at high latitudes the modal age is younger in summer than other seasons. This summer shortcut can also be clearly seen at 420 K, especially in the NH. For instance, it takes only 2 months to transport the spectral peak from the TTL to the NH high latitudes during June–August. But this

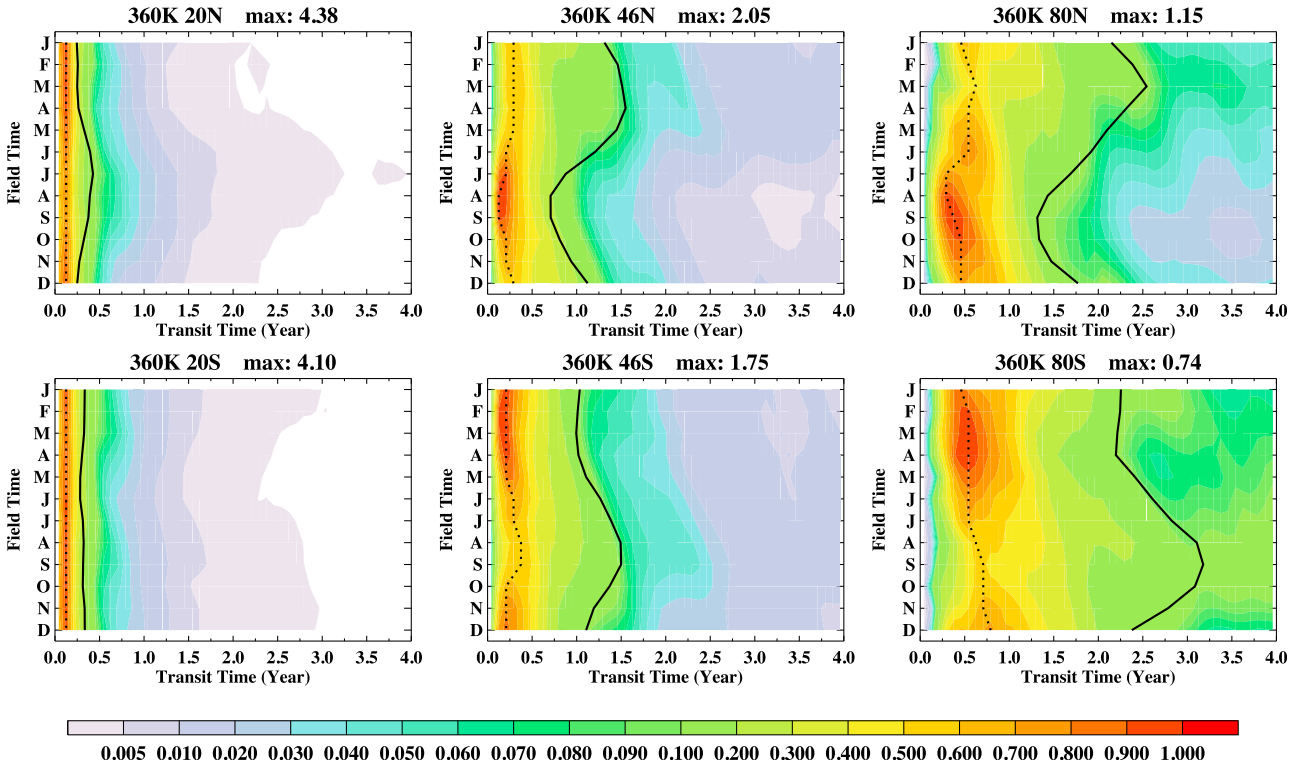

Figure 8. Seasonal cycle of the age spectra at 20°, 46°, and 80° latitude north and south at 360 K. The dotted line is the modal age, and the solid line is the mean age. The colors are normalized by the maximum probability density function shown in the caption.

fast path is shut off during winter–early spring, as illustrated by the strong gradients in the subpolar latitudes. These large gradients, also seen in the mean age, show the change of the relative importance of the fast isentropic mixing and the slow Brewer-Dobson circulation descent in winter–early spring due to the combined effect of the strong wintertime adiabatic descent and the polar barrier. The modal age at 550 K shows very dramatic seasonal variations at high latitudes. Interestingly the strongest gradient in the mean age occurs in the subtropics, representing the impact of the subtropical barrier that isolates the tropical pipe from the surf zone. However, the subtropical barrier is not as clear in the modal age.

[34] We now examine the seasonal cycle of the age spectra at different latitudes on the 360, 420, and 550 K isentropic surfaces. At 360 K and 20°N a narrow spectral peak at 1 month characterizes the age spectra (Figure 8). The modal ages are the same for all seasons, but the width is wider in summer than in winter. At 46°N, the strongest spectral peaks and the youngest peak value (1 month) occur in August and September. The weakest peaks (about half that in fall) with the oldest peak values (3 months) occur in March and April, suggesting that the fast pathway evident during the summer is suppressed during the winter. Almost exactly the same seasonal variations are found at high latitudes. At 80°N, the fall age spectra have the youngest mean age and the strongest spectral peak. Their modal age of 4–5 months indicates that the spectral peaks leave the source region in late spring–early summer. The spring spectra have the oldest mean and modal age, and their spectral peaks are traced back to fall of the previous year. These results are consistent with the wintertime tropospheric jet barrier in the lowermost stratosphere. The SH age spectra have very similar seasonal variability as their NH counterparts.

[35] The overall seasonal change in the age spectra at the 420 K isentropic surface (Figure 9) is similar to that at 360 K. One feature in the 420 K age spectra not seen in the lowermost stratosphere is the large change in the modal age at high latitudes (also see Figure 7e). For instance at 80°S the modal age changes dramatically from about 0.75 years in the February spectrum to about 4 years in the November spectrum. The sharp jump in the modal age is associated with significant changes in the spectral shape. For example, the February and March spectra at 80°N have three comparable peaks with transit time of about 1.2, 2.7, and 3.7 years, respectively. The second peak is a bit higher than the other two and that is the modal age by definition. Apparently the modal age is not a very useful parameter to characterize the spectral shape for this kind of spectrum. Note even the first peak is much older than the 0.5 year modal age of the summer spectra. Also the magnitude of the February–March peaks is about 1/4 of the July–August spectra. We interpret this as the seasonal change of the dominant pathway at high latitudes. In summer–early fall, isentropic mixing brings young TTL air directly to the polar region. In winter-spring, slow descent from high altitude dominates.

[36] The 550 K age spectra also show large jumps in modal age at high latitudes (Figure 10). The modal ages of the winter-spring spectra are much older (up to two times) than those of the summer spectra, but the magnitudes of the spectral peaks are greater in winter-spring than in summer. This suggests that mixing between middle and high latitudes in summer, which is weak because of the summer

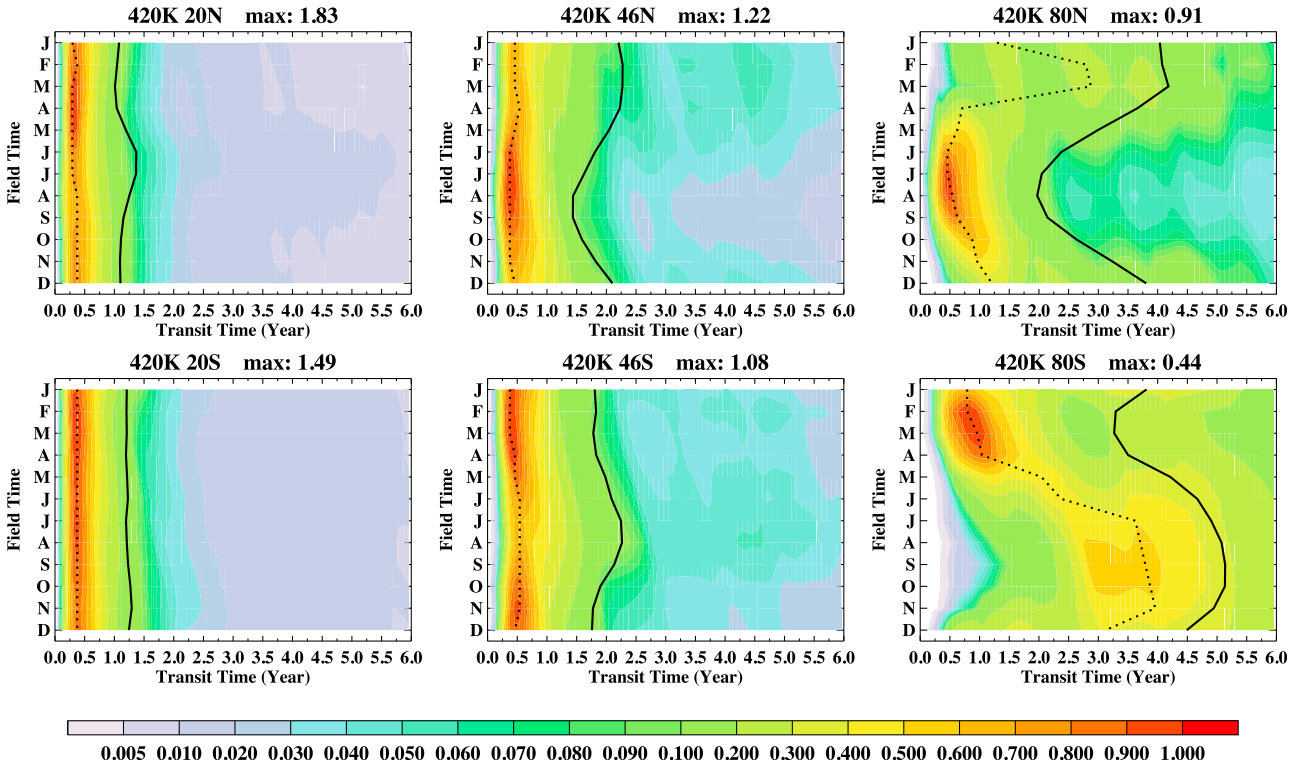

Figure 9. Same as Figure 8 but for 420 K.

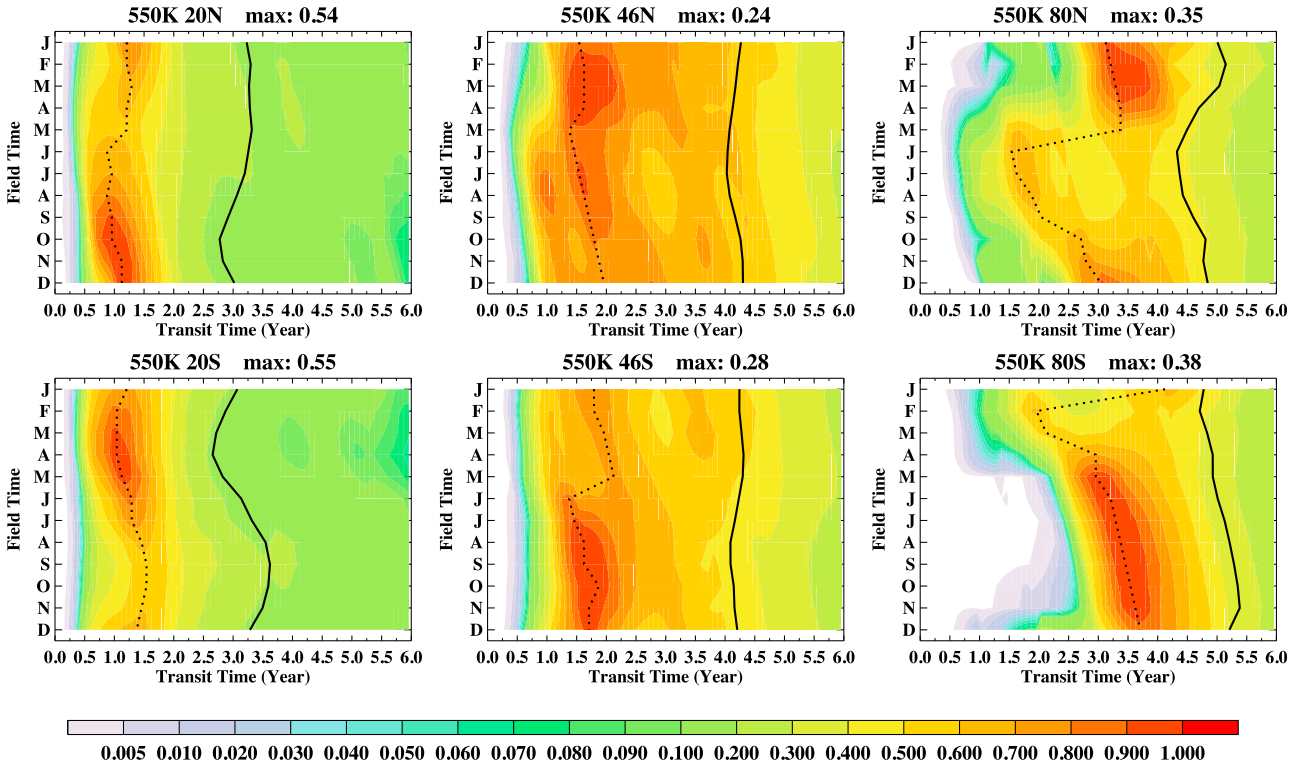

Figure 10. Same as Figure 8 but for 550 K.

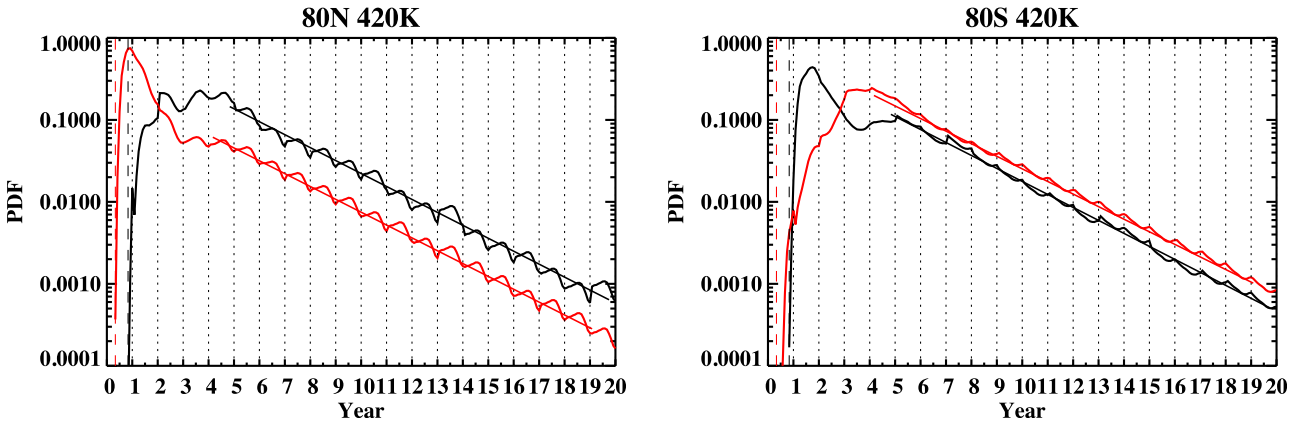

Figure 11. The March (black) and September (red) age spectra at 80 N and 80 S at 420 K. The starting points of the age spectra are shifted (indicated by the dashed lines) so that the *x* axis represents the season of the source time. The vertical dotted lines correspond to January in source time.

stratospheric easterlies, leads to a younger although weaker spectral peak in the polar region. In winter-spring the mixing is prohibited and the spectral peaks represent solely the descent of the Brewer-Dobson circulation.

[37] The change of the spectral shape from a single peak at low and middle latitudes to multiple peaks at high latitudes was first reported by *Reithmeier et al.* [2008], who calculated age spectra in the ECHAM4 GCM using the Lagrangian trajectory method. A major focus of *Reithmeier et al.* [2008] was to understand what causes the high latitudes multiple spectral peaks, which are 1 year apart and independent of height. They argued that these multimodal polar spectra are caused by two processes: the seasonality of the tropical upwelling that generates single mode spectra at midlatitudes, and the summertime mixing between the polar and midlatitude air that leads to a superposition of the midlatitude single mode spectra with the polar spectra once a year and generates multiple annual peaks.

[38] Although our age spectra show multiple peaks similar to those of *Reithmeier et al.* [2008], there are some differences. Figure 11 shows the March and September age spectra at 80 N and 80 S at 420 K. The starting points of the age spectra are shifted such that the *x* axis reflects the season of the source time. The age spectra are plotted in the logarithmic scale to highlight the tail region. In both the NH and SH high latitudes, the annually repeating peaks last contacted the tropical surface during their respective summer season. This is not the case in the work of *Reithmeier et al.* [2008]. These annual peaks are very clear in the tail region, suggesting they are caused by the annual cycle of the recirculation into the polar stratosphere. Our results indicate that air parcels leaving the tropical surface in summer have a larger chance to be recirculated into the polar stratosphere. The annual cycle of the Brewer-Dobson circulation and polar vortex barrier appear to determine the annual cycle of the recirculation into the polar region, but the mechanism is not clear.

[39] The tails of the age spectra, defined here as regions with transit time older than 4 years, decay exponentially with time. Thus the tails can be approximated by an exponentially decaying mode $\Psi_0(r, t)\exp(\xi/\tau_0)$ (straight solid lines in Figure 11). This decay rate τ_0 is the eigentime of the lowest mode of the age spectra [*Hall et al.*, 1999a; *Ehhalt et al.*, 2004]. Physically it describes how fast transport alone causes the eventually decay of the mixing ratio of a conserved tracer in the stratosphere [*Ehhalt et al.*, 2004]. It is a fundamental stratospheric transport diagnostic and remains nearly constant in different seasons and locations (2.77 years in the GEOSCCM). Of course this does not mean that the tails are not seasonally dependent, because $\Psi_0(r,t)$ changes with season and location.

5. Discussion and Summary

[40] The differences between the age spectrum and the BIR are known in tropospheric and ocean transport studies [*Holzer et al.*, 2003; *Haine et al.*, 2008], but the BIR is often used as the age spectrum in stratospheric transport [*Hall and Plumb*, 1994; *Hall et al.*, 1999a, 1999b; *Schoeberl et al.*, 2005]. These studies perform a single pulse tracer experiment and the resultant BIR is used as an approximation of the time-averaged age spectrum. Here we show that the BIRs have significant seasonal variations. Thus it is problematic to use a single BIR realization to represent the annually averaged age spectrum. Our model results also show that the seasonal cycle of the BIRs is different from that of the age spectra. Clearly it is misleading to use BIRs to study the seasonality of the age spectra. On the other hand, *Haine et al.* [2008] showed theoretically that an ensemble-averaged BIR is equivalent to an ensemble-averaged age spectrum. This is confirmed by the nearly identical annually averaged BIR and age spectrum in our results (not shown). In summary, computing an ensemble of BIRs is needed in order to investigate either the seasonality or the annual-mean properties of the age spectra.

[41] Age spectra in the GEOSCCM have significant seasonal variations throughout the stratosphere caused by the presence of seasonal transport barriers. The largest seasonal changes occur in the lowermost and lower stratosphere and the subtropical overworld. Up to 40% differences between the individual month and annually averaged mean age are commonly found in these regions. The modal ages and spectral shapes demonstrate even bigger changes in the polar stratosphere. The seasonal variations of the age spectra

reflect the seasonal evolution and relative importance of the slow Brewer-Dobson circulation and the fast isentropic mixing.

[42] We have shown that 12 BIRs are sufficient to reconstruct seasonally varying age spectra under the cyclostationarity assumption. To examine whether the seasonal cycle of the age spectra could be properly captured using even fewer BIRs we calculate age spectra using two BIRs (every 6 months), four BIRs (every 3 months) and six BIRs (every 2 months) and compare them with the age spectra calculated from the full 12 BIRs (figure not shown). The age spectra derived from two BIRs have a wrong seasonal cycle in the tropical and midlatitude lower stratosphere. The age spectra computed from four BIRs capture most of the seasonal features of the mean age and spectral width, but they cannot resolve the young modal ages in the tropical-subtropical lowermost stratosphere and significantly underestimate the magnitudes of spectral peaks in this region. Only the age spectra computed from six BIRs reproduce nearly the same season cycle as that from the full 12 BIRs. Thus at least six BIRs are needed in order to correctly capture the seasonal variability of the age spectra.

[43] Several studies have used empirical age spectra to investigate stratospheric transport [*Andrews et al.*, 1999, 2001a; *Bönisch et al.*, 2009]. They assumed an analytic solution for the age spectra and used in situ trace gas measurements to constrain the empirical parameters. *Andrews et al.* [2001a] proposed a bimodal spectral shape with two distinct peaks to represent the fast quasihorizontal mixing and slow Brewer-Dobson circulation in the NH midlatitude lower stratosphere, respectively. *Bönisch et al.* [2009] adopted this bimodal concept and made the important revision that the superposition of the two modes does not necessarily lead to two distinct spectral peaks. The age spectra in the GEOSCCM show a single peak in this region (see Figures 8 and 9), which does not support the bimodal shape of *Andrews et al.* [2001a]. Our results appear to be consistent with the conceptual model of *Bönisch et al.* [2009]. However, *Bönisch et al.* [2009] concentrated on the mean age and did not present the seasonal evolution of their empirical age spectra. Therefore we could not make direct comparisons with *Bönisch et al.* [2009]. We do find multimodal spectral shapes at high latitudes, but the multiple spectral peaks are due to the annual cycle of air recirculation. As pointed out by *Reithmeier et al.* [2008], it is very challenging to apply this multimodal spectral shape in empirical studies.

[44] In our 20 year model simulation the stratospheric transport does not have a statistically significant trend, but on a longer time scale the secular trend in stratospheric transport has been shown to be important in CCM simulations [e.g., *Butchart et al.*, 2010]. It is an outstanding scientific question how future changes in stratospheric transport will impact long-term changes in mean age and age spectra. The GESOCCM, like other CCMs, consistently simulates a decrease of the stratospheric mean age by about 20% in the 21st century [e.g., *Oman et al.*, 2009; *Butchart et al.*, 2010]. It is well known that decreasing mean age in a warming climate is strongly correlated with increased tropical upwelling [*Austin and Li*, 2006; *Li et al.*, 2008; *Garcia and Randel*, 2008]. It is not clear how changes in other processes such as mixing will impact the long-term changes in mean age. Investigating the long-term changes in age spectra will identify the relative importance of changes in tropical upwelling and mixing-recirculation to changes in mean age. For example, changes in the spectral width and the tail decay rate τ_0 are closely related to changes in mixing and recirculation, whereas changes in the modal age reflect those in the mean advection of the Brewer-Dobson circulation. We will investigate the long-term changes in the stratospheric age spectra in the 21st century in a separate study.

[45] **Acknowledgments.** This work is supported by NASA's Modeling, Analysis, and Prediction program. We thank Laura Pan for very helpful discussions. Computational resources for this work were provided by NASA's High-Performance Computing through the generous award of computing time at NASA Ames Research Center.

References

Andrews, A. E., K. A. Boering, B. C. Daube, S. C. Wofsy, E. J. Hintsa, E. M. Weinstock, and T. P. Bui (1999), Empirical age spectra for the lower tropical stratosphere from in situ observations of CO_2: Implications for stratospheric transport, *J. Geophys. Res.*, *104*, 26,581–26,595, doi:10.1029/1999JD900150.

Andrews, A. E., K. A. Boering, S. C. Wofsy, B. C. Daube, D. B. Jones, S. Alex, M. Loewenstein, J. R. Podolske, and S. E. Strahan (2001a), Empirical age spectra for the midlatitude lower stratosphere from in situ observations of CO_2: Quantitative evidence for a subtropical "barrier" to horizontal transport, *J. Geophys. Res.*, *106*, 10,257–10,274, doi:10.1029/2000JD900703.

Andrews, A. E., K. A. Boering, S. C. Wofsy, B. C. Daube, D. B. Jones, S. Alex, M. Loewenstein, J. R. Podolske, and S. E. Strahan (2001b), Mean ages of stratospheric air derived from in situ observations of CO_2, CH_4, and N_2O, *J. Geophys. Res.*, *106*, 32,295–32,314, doi:10.1029/2001JD000465.

Austin, J., and F. Li (2006), On the relationship between the strength of the Brewer-Dobson circulation and the age of stratospheric air, *Geophys. Res. Lett.*, *33*, L17807, doi:10.1029/2006GL026867.

Bönisch, H., A. Engel, J. Curtius, T. Birner, and P. Hoor (2009), Quantifying transport into the lowermost stratosphere using simultaneous in-situ measurements of SF_6 and CO_2, *Atmos. Chem. Phys.*, *9*, 5905–5919, doi:10.5194/acp-9-5905-2009.

Butchart, N., et al. (2010), Chemistry-climate model simulations of twenty-first century stratospheric climate and circulation change, *J. Clim.*, *23*, 5349–5374, doi:10.1175/2010JCLI3404.1.

Chen, P. (1995), Isentropic cross-tropopause mass exchange in the extratropics, *J. Geophys. Res.*, *100*, 16,661–16,673, doi:10.1029/95JD01264.

Douglass, A. R., C. J. Weaver, R. B. Rood, and L. Coy (1996), A three dimensional simulation of the ozone annual cycle using winds from a data assimilation system, *J. Geophys. Res.*, *101*, 1463–1474, doi:10.1029/95JD02601.

Ehhalt, D. H., F. Rohrer, S. Schauffler, and M. Prather (2004), On the decay of stratospheric pollutants: Diagnosing the longest-lived eigenmode, *J. Geophys. Res.*, *109*, D08102, doi:10.1029/2003JD004029.

Eyring, V., et al. (2006), Assessment of temperature, trace species, and ozone in chemistry-climate model simulations of the recent past, *J. Geophys. Res.*, *111*, D22308, doi:10.1029/2006JD007327.

Garcia, R. R., and W. Randel (2008), Acceleration of the Brewer-Dobson circulation due to increases in greenhouse gases, *J. Atmos. Sci.*, *65*, 2731–2739, doi:10.1175/2008JAS2712.1.

Haine, T. W. N., H. Zhang, D. W. Waugh, and M. Holzer (2008), On transit-time distributions in unsteady circulation models, *Ocean Modell.*, *21*, 35–45, doi:10.1016/j.ocemod.2007.11.004.

Hall, T. M., and R. A. Plumb (1994), Age as a diagnostic of stratospheric transport, *J. Geophys. Res.*, *99*, 1059–1070, doi:10.1029/93JD03192.

Hall, T. M., D. J. Wuebbles, K. A. Boering, R. S. Eckman, J. Lerner, R. A. Plumb, D. H. Rind, C. P. Rinsland, D. W. Waugh, and C.-F. Wei (1999a), Transport experiments, *NASA Tech. Memo.*, *NASA TM-1999-209554*, 110–189.

Hall, T. M., D. W. Waugh, K. A. Boering, and R. A. Plumb (1999b), Evaluation of transport in stratospheric models, *J. Geophys. Res.*, *104*, 18,815–18,839, doi:10.1029/1999JD900226.

Holzer, M., I. G. McKendry, and D. A. Jaffe (2003), Springtime trans-Pacific atmospheric transport from east Asia: A transit-time probability density function approach, *J. Geophys. Res.*, *108*(D22), 4708, doi:10.1029/2003JD003558.

Intergovernmental Panel on Climate Change (2001), *Climate Change 2001: The Scientific Basis. Contribution of Working Group 1 to the Third*

Assessment Report, edited by J. T. Houghton et al., Cambridge Univ. Press, New York.

Khatiwala, S., F. Primeau, and T. Hall (2009), Reconstruction of the history of anthropogenic CO_2 concentrations in the ocean, *Nature*, *462*, 346–349, doi:10.1038/nature08526.

Li, F., J. Austin, and J. Wilson (2008), The strength of the Brewer-Dobson circulation in a changing climate: Coupled chemistry-climate model simulations, *J. Clim.*, *21*, 40–57, doi:10.1175/2007JCLI1663.1.

Oman, L., D. W. Waugh, S. Pawson, R. S. Stolarski, and P. A. Newman (2009), On the influence of anthropogenic forcings on changes in the stratospheric mean age, *J. Geophys. Res.*, *114*, D03105, doi:10.1029/2008JD010378.

Pan, L., S. Solomon, W. Randel, J.-F. Lamarque, P. Hess, J. Gille, E.-W. Chiou, and M. P. McCormick (1997), Hemispheric asymmetries and seasonal variations of the lowermost stratospheric water vapor and ozone derived from SAGE II data, *J. Geophys. Res.*, *102*, 28,177–28,184, doi:10.1029/97JD02778.

Pawson, S., R. S. Stolarski, A. R. Douglass, P. A. Newman, J. E. Nielsen, S. M. Frith, and M. L. Gupta (2008), Goddard Earth Observing System chemistry climate model simulations of stratosphere ozone temperature coupling between 1950 and 2005, *J. Geophys. Res.*, *113*, D12103, doi:10.1029/2007JD009511.

Randel, J. W., F. Wu, A. Gettelman, J. M. Russell III, J. M. Zawodnya, and S. J. Oltmans (2001), Seasonal variation of water vapor in the lower stratosphere observed in Halogen Occultation Experiment data, *J. Geophys. Res.*, *106*, 14,313–14,325, doi:10.1029/2001JD900048.

Ray, E. A., F. L. Moore, J. W. Elkins, G. S. Dutton, D. W. Fahey, H. Vomel, S. J. Oltmans, and K. H. Rosenlof (1999), Transport into the Northern Hemisphere lowermost stratosphere revealed by in situ tracer measurements, *J. Geophys. Res.*, *104*, 26,565–26,580, doi:10.1029/1999JD900323.

Reithmeier, C., R. Sausen, and V. Grewe (2008), Investigating lower stratospheric model transport: Lagrangian calculation of mean age and age spectra in the GCM ECHAM4, *Clim. Dyn.*, *30*, 225–238, doi:10.1007/s00382-007-0294-1.

Rienecker, M. M., et al. (2008), The GEOS-5 data assimilation system—Documentation of versions 5.0.1, 5.1.0, and 5.2.0, *NASA Tech. Memo.*, *NASA TM-2008-104606*, vol. 27, 118 pp.

Rosenlof, K. H. (1995), Seasonal cycle of the residual mean meridional circulation in the stratosphere, *J. Geophys. Res.*, *100*, 5173–5191, doi:10.1029/94JD03122.

Rosenlof, K. H., A. F. Tuck, K. K. Kelly, J. M. Russell III, and M. P. McCormick (1997), Hemispheric asymmetries in water vapor and inferences about transport in the lower stratosphere, *J. Geophys. Res.*, *102*, 13,213–13,234, doi:10.1029/97JD00873.

Schoeberl, M. R., A. R. Douglass, Z. Zhu, and S. Pawson (2003), A comparison of the lower stratospheric age spectra derived from a general circulation model and two data assimilation systems, *J. Geophys. Res.*, *108*(D3), 4113, doi:10.1029/2002JD002652.

Schoeberl, M. R., A. R. Douglass, B. Polansky, C. Boone, K. A. Walker, and P. Bernath (2005), Estimation of stratospheric age spectrum from chemical tracers, *J. Geophys. Res.*, *110*, D21303, doi:10.1029/2005JD006125.

Strahan, S. E., M. R. Schoeberl, and S. D. Steenrod (2009), The impact of tropical recirculation of polar composition, *Atmos. Chem. Phys.*, *9*, 2471–2480, doi:10.5194/acp-9-2471-2009.

Strahan, S. E., et al. (2011), Using transport diagnostics to understand chemistry climate model ozone simulations, *J. Geophys. Res.*, *116*, D17302, doi:10.1029/2010JD015360.

Waugh, D. W., and T. M. Hall (2002), Age of stratospheric air: Theory, observations, and models, *Rev. Geophys.*, *40*(4), 1010, doi:10.1029/2000RG000101.

Waugh, D. W., T. M. Hall, and T. W. N. Haine (2003), Relationships among tracer ages, *J. Geophys. Res.*, *108*(C5), 3138, doi:10.1029/2002JC001325.

Waugh, D. W., T. W. N. Haine, and T. M. Hall (2004), Transport times and anthropogenic carbon in the subpolar North Atlantic Ocean, *Deep Sea Res., Part I*, *51*, 1475–1491.

World Meteorological Organization (2007), Scientific assessment of ozone depletion: 2006, *Global Ozone Res. Monit. Project Rep. 50*, 572 pp., Geneva, Switzerland.

A. R. Douglass, P. A. Newman, J. E. Nielsen, S. Pawson, and R. S. Stolarski, NASA Goddard Space Flight Center, Greenbelt, MD 20771, USA.

F. Li and S. E. Strahan, NASA Goddard Earth Sciences Technology and Research, Greenbelt, MD 20771, USA. (feng.li@nasa.gov)

D. W. Waugh, Department of Earth and Planetary Science, Johns Hopkins University, 3400 N. Charles St., Olin Hall 321, Baltimore, MD 21218, USA.